

## The Temporal Resolution Limit of the Silicon Image Sensors

Takeharu Goji Etoh<sup>1,2\*</sup>, Anh Quang Nguyen<sup>1</sup>, Yoshinari Kamakura<sup>2</sup>,  
Kazuhiro Shimonomura<sup>1</sup>, Yen Le Thi<sup>2</sup> and Nobuya Mori<sup>2</sup>

<sup>1</sup> Graduate School of Science and Engineering, Ritsumeikan University, Noji-Higashi, Kusatsu, 525-8577 Japan

<sup>2</sup> Graduate School of Engineering, Osaka University, 2-1 Yamada-Oka, Suita, Osaka 565-0871 Japan

\* Correspondent author: yb6t-etu@asahi-net.or.jp; Tel.: +81-(0)90-1901-4429

### Abstract

Rayleigh proposed a spatial resolution limit when resolution of lenses approached to the limit. The frame rate of image sensors has been exponentially increasing. A simulation study showed a silicon image sensor can achieve the frame interval less than 200 ps (about  $10^{10}$  fps) with an existing 130 nm technology. It's time to search the ultimate high speed. An expression of the theoretical highest frame rate of silicon image sensors is derived. For example, the temporal resolution limit for green light of 550 nm is 11.1 picoseconds; the inverse, the theoretical highest frame rate is 90.1 Gfps (about  $10^{11}$  fps).

### 1. Acceleration of the Frame Rate

Fig. 1 shows the evolution of high-speed imaging devices. The blue squares and the green circles show the highest frame rate recorded by cameras with high-speed silicon image sensors. The blue squares indicate the frame rates achieved by standard high-speed cameras with one silicon image sensor. The green circles represent cameras with a set of multiple cameras or image sensors and a camera with an image sensor with macro-pixels each consisting of multiple pixels operated as a group. The red triangles indicate the frame rates recorded with imaging devices supported by technologies other than high-speed image sensors. The size of each plot represents the frame counts. The squares drawn with the blue solid and the blue dashed lines respectively show the frame rates of silicon image sensors under process and those under design.

As cameras with the silicon image sensors are compact, sensitive and user-friendly, their performance has been rapidly improved. For example, the highest frame rate has been exponentially increased (a linear increase in a semi-logarithmic scale in Fig. 1). A simulation study predicted that the frame interval less than 200 ps (about  $10^{11}$  fps) can be achieved with existing process technology [1]-[3]. On the other hand, the frame rates of other continuous imaging devices mostly stay at  $10^{11}$  to  $10^{12}$  fps.

The highest frame rate of the cameras with silicon image sensors has come closer to the frame rate achievable only by other high-speed imaging devices in the past. The spatial resolution limit was discussed by Abbe, Rayleigh, etc., when the resolution of lenses approached the limit. It is time to search for the temporal resolution limit of the image sensors.

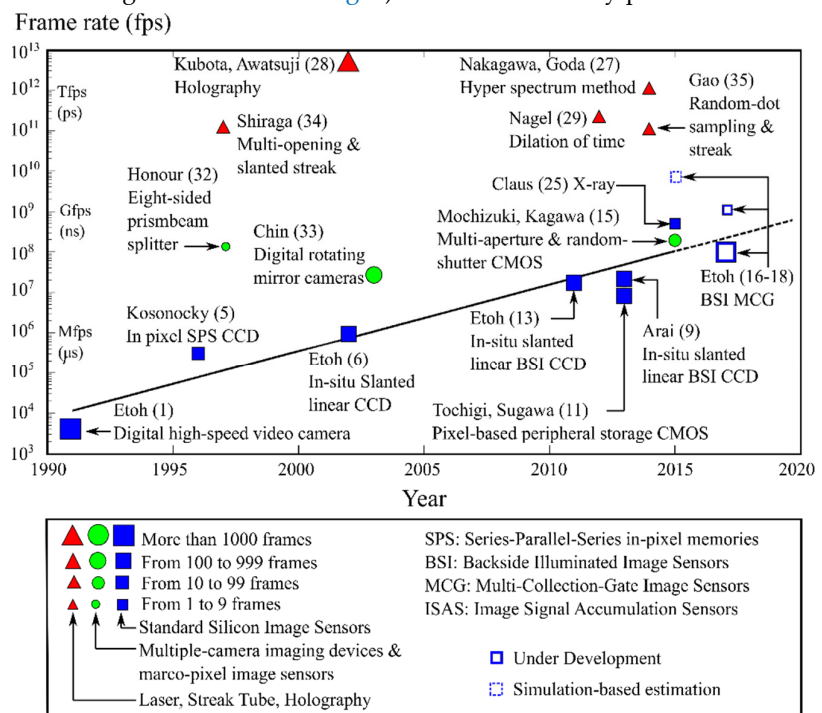


Fig. 1 Evolution of high-speed imaging devices (Refer to [3] for the numbers in the figure.)

## 2. Logic for the Derivation

The derivation includes the following logical steps. The reasons are explained in figures.

- (1) The camera has one image sensor and each pixel of the sensor independently detects incident light.
- (2) Temporal resolution of the image sensor is limited by the motion of signal electrons. That of the detection circuit is assumed to be infinitesimal.
- (3) A photon group instantly arrives at a pixel of the image sensor. Two of the photon groups arrive with the time interval of  $\Delta\tau$ . Two batches of electrons generated by the two photon groups travel in the sensor layer to a detection plane, keeping the interval of  $\Delta\tau$ .
- (4) The distribution of the travel time of each electron batch detected at the detection plane can be approximated by the Gaussian distribution for the first order approximation.
- (5) Effects of horizontal drift and diffusion to the travel time distribution can be reduced by design efforts (Fig. 2). There remain two unavoidable factors affecting the distribution: (a) *mixing* of signal electrons with different vertical travel distances due to distributing penetration depths of photons; (b) *pure diffusion* due to random motions of electrons (Fig. 3).
- (6) Expressions of variances  $\sigma_m^2$  and  $\sigma_d^2$  of the travel time respectively caused by the vertical mixing and the diffusion are separately derived and added (Eq. 1 to Eq. 8), since they are independent processes.
- (7) The no-dip condition for two superposed Gaussian distributions is employed as the separation condition of the arrival time distributions of the electron batches, which is precisely  $2\sigma (= \Delta\tau)$ , where  $\sigma$  is the standard deviation of one Gaussian distribution (Fig. 4, Eq. 9). In this case,  $\sigma^2 = \sigma_m^2 + \sigma_d^2$ .
- (8) The expression includes the thickness of the layer  $W$ , the drift velocity  $v$ , the diffusion coefficient  $D$ , and the average penetration depth  $\delta$ . To calculate the temporal resolution limit, reasonable values of these parameters should be selected and substituted to the derived expressions.
- (9) Eq. 9 is minimized for a larger  $v$  and a smaller  $D$ . Both decrease for a higher concentration. As observed in Eq. 9, the effect of  $v$  is dominant. Therefore, the intrinsic silicon layer is assumed.
- (10) The temporal resolution  $2\sigma$  is minimized by the values of  $v$  and  $D$  at the critical field,  $2.5 \times 10^4$  V/cm, where the critical field corresponding to the field to which the diffusion coefficient is minimized before increasing again due to secondary electrons generated by the high field (Fig. 5).
- (11) Eq. 9 is verified by comparison with Monte Carlo simulations for the values of  $v$  and  $D$  for the critical field (Fig. 6).
- (12) The thickness  $W$  is assumed to be equal to the average penetration depth  $\delta$ . For  $W < \delta$ , the sensitivity decreases due to loss of photons penetrating the whole thickness  $W$ , and, for  $W > \delta$ , the temporal resolution increases due to the long travel distance. Therefore,  $W' = W/\delta = 1$  (Eq. 10).
- (13) Monte Carlo simulations show  $\sigma_m \gg \sigma_d$  for ranges of  $W$  in practical applications (Fig. 6). When the diffusion effect  $\sigma_d$  is neglected, the expression of the temporal resolution limit can be further reduced to an extremely simple form (Eq. 11). The relative error of Eq. (11) to Eq. (10) is 4 % for the green light.
- (14) For green light of 550 nm and the critical field to the intrinsic silicon layer, the temporal resolution limit is 11.1 ps from Eq. (10), which is equivalent to 90.1 Gfps.

## 3. Derivation of the Standard Deviation of the Travel Time

The effect of the horizontal travel of electrons can be suppressed by design efforts, such as implementing a micro-lens/a light guide, thinning the chip and optimizing the p-well shape. However, the diffusion due to the random motion and the mixing due to the distribution of the penetration depth are unavoidable. The two effects are included in a simplified electron travel model shown in Fig. 3. Fig. 3(b) shows sample trajectories of five generated electrons.

In Fig. 3(b), the travel distance of an electron generated at the depth  $s$  from the backside to the front side is  $(W-s)$ , and the average travel time  $t_r$  is  $(W-s)/v$ .

The probability density of the penetration depth  $s$  is expressed by the exponential distribution  $f(s)$  (Eq.1). The zeroth to the second moments of the average travel time are expressed by Eq. 2 to Eq. 4. Then, the variance  $\sigma_m^2$  due to the mixing effect of electrons penetrating to different depths is expressed by Eq. 5. After some cumbersome manipulation of equations, the expression for  $\sigma_m^2$  was fortunately reduced to a relatively simple form Eq. 6, where  $W' = W/\delta$ .

The random motion of signal electrons is superposed on the drift motion. The solution of the drift and diffusion equation shows that, when the travel time increases, the travel time distribution

approaches the Gaussian distribution with the average travel time is  $t_r$  and the variance is  $2D/v^2$ . Therefore, the variance is proportional to  $t_r$  multiplied by  $2D/v^2$ . The average travel time  $t_r$  distributes due to the distribution of the penetration depth of light. Therefore, the variance  $\sigma_d^2$  due to the diffusion effect is given by integration of the variance conditional to the average travel time weighted by the distribution of the penetration depth as shown in Eq. 7.

The mixing due to the distribution of the penetration depth and the diffusion conditioned by the average travel time are independent processes. Therefore, the total variance  $\sigma_s^2$  is the sum of  $\sigma_m^2$  and  $\sigma_d^2$  as shown in Eq. 8. Then, the temporal resolution limit is expressed by Eq. 9. When  $W' = W/\delta = 1$ , it is reduced to Eq. 10, and, when the diffusion effect is neglected, it is further reduced to Eq. 11.

#### 4. Monte Carlo Simulation

The model is explained in Fig. 3(a). The total thickness is 30  $\mu\text{m}$ . At the back and the front sides, 5  $\mu\text{m}$ -thick buffer layers are excluded from the Monte Carlo simulation to avoid the boundary-layer effects.

Photons are incident to the plane at the distance of 25  $\mu\text{m}$  from the bottom. The detection plane is set at 5  $\mu\text{m}$  from the bottom at first, and elevated to 24.9  $\mu\text{m}$  to calculate the standard deviation of the travel time for the different  $W$ . Thus, the thickness is changed from 20  $\mu\text{m}$  ( $2 \times 10^{-3}$  cm) to 0.1  $\mu\text{m}$  ( $1 \times 10^{-5}$  cm).

The drift velocity  $v$  and the diffusion coefficient  $D$  are set at the values for the critical field of the intrinsic silicon. For the Monte Carlo simulations, an advanced model based on the full band calculations is employed. Basic parameters on the motion of charges can be calculated by the simulation method, including the drift velocity  $v$  and the diffusion coefficient  $D$ . In Fig. 5, two values are given both for  $v$  and  $D$ . One set of the values are estimated based on the curves given by experiments: the others are calculated by this Monte Carlo simulation model. Practically, they agree well. For confirmation of the accuracy of the derived expression, the values of  $v$  and  $D$  calculated by the Monte Carlo simulation is used for consistency in the calculations.

Fig. 6 shows the temporal resolution  $2\sigma_s$  plotted against the thickness  $W$ . The solid lines and the dots respectively indicate the results calculated from Eq. 9 and by the Monte Carlo simulations. They agree almost perfectly for the thickness larger than 1  $\mu\text{m}$  ( $10^{-4}$  cm).

Another important observation is that the mixing effect  $2\sigma_m$  is dominant over the diffusion effect  $2\sigma_d$ , validating the approximation of Eq. 11. The values estimated by Eq. 10 and Eq. 11 are respectively 12.4 ps and 12.0 ps for the green light. The error is less than 4%.

Experimental data of the drift velocity and the diffusion coefficient at the critical field are slightly different from those estimated by the Monte Carlo simulation as shown in Fig. 5. By substituting these values into Eq. 10, the temporal resolution limit for green light of 550 nm is calculated as 11.1 ps. The inverse, the upper-bound frame rate, is 90.1 fps (about  $10^{11}$  fps).

**References** 1) V. T. S. Dao et al., Toward 10 Gfps: Factors Limiting the Frame Rate of the BSI Image Sensor, Proc. IISW2015, 2015. 2) C. Zhang, et al., Pixel parallel, localized driver design for a 128 x 256 pixel array 3D 1Gfps image sensor, Selected Papers from the 31st ICHSIP, Proc. of SPIE10328, 1032807, 2016. 3) T. G. Etoh, et al., The Theoretical Highest Frame Rate of Silicon Image Sensors, *Sensors*, 17(3), 483, 2017.

$$f(s) = (1/\delta) \exp(-s/\delta) \quad (1)$$

$$p = \int_0^W f(s) ds = 1 - \exp(-W/\delta) \quad (2)$$

$$E(t_r) = \int_0^W \{(W-s)/v\} f(s)/p ds = (W - \delta p)/(vp) \quad (3)$$

$$E(t_r^2) = \int_0^W \{(W-s)/v\}^2 f(s)/p ds \\ = (W^2 - 2W\delta + 2\delta^2)/v^2 + \frac{W^2 - 2W\delta}{v^2 p} \exp(-W/\delta) \quad (4)$$

$$\sigma_m^2 = E(t_r^2) - [E(t_r)]^2 \quad (5)$$

$$\sigma_m^2 = \frac{W^2}{p^2 v^2} [-\exp(-W/\delta) + \frac{\delta^2}{W^2} p^2] - \frac{\delta^2 W^2}{p^2 v^2} \exp(-W/\delta) + \frac{\delta^2}{v^2} \quad (6)$$

$$\sigma_d^2 = \frac{2D}{v^2} E(t_r) = \frac{2D}{v^2} \int_0^W \{(W-s)/v\} f(s)/p ds = \frac{(W-p) 2D \delta}{p v^2 v} \quad (7)$$

$$\sigma_s^2 = \sigma_m^2 + \sigma_d^2 \quad (8)$$

$$\Delta\tau = 2\sigma_s = 2\sqrt{\sigma_m^2 + \sigma_d^2} = 2\sqrt{\left[ -\frac{\delta^2 W^2}{p^2 v^2} \exp(-W/\delta) + \frac{\delta^2}{v^2} \right] + \left[ \frac{(W-p) 2D \delta}{p v^2 v} \right]} \quad (9)$$

$$\Delta\tau = 2\sqrt{0.079 \frac{\delta^2}{v^2} + 0.582 \frac{2D \delta}{v^2 v}} \quad (10) \quad \Delta\tau = 0.562 \frac{\delta}{v} \quad (11)$$

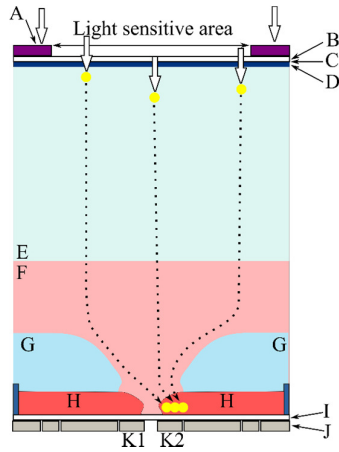


Fig. 2 A cross-section of a BSI image sensor: electrons travel in the vertical and horizontal directions. While the horizontal motion is dominant on the travel time, the effect can be reduced by design efforts.

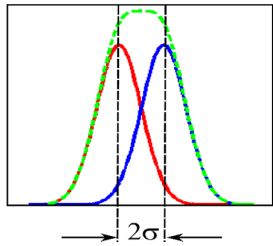


Fig. 4 No-dip condition for superposed Gaussian distributions  
 $\mu_2 - \mu_1 = 2\sigma$ ;  $\mu$ : average,  
 $\sigma$ : standard deviation

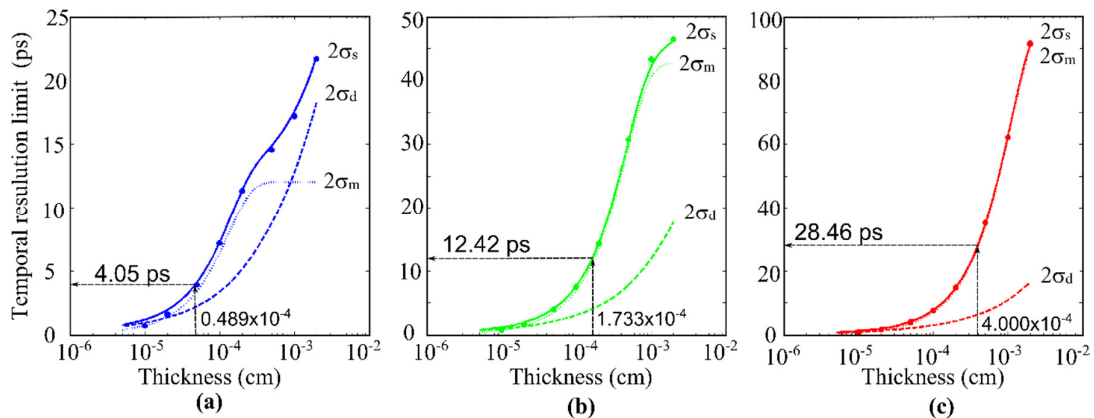


Fig. 6 The derived expression of the temporal resolution limit vs. Results of Monte Carlo simulations. Solid lines: the temporal resolution limit  $2\sigma_s$ , Eq. 9; Dots: the Monte Carlo simulation Results Dotted lines: the mixing effect  $2\sigma_m$  (the first component of Eq. 9; Dashed lines: the diffusion effect  $2\sigma_d$ , the second component of Eq. 9. Intrinsic silicon <111>; 300 K; Electric field:  $2.5 \times 10^4$  V/cm; Wavelength: (a) 450 nm, (b) 550 nm, (c) 650 nm.

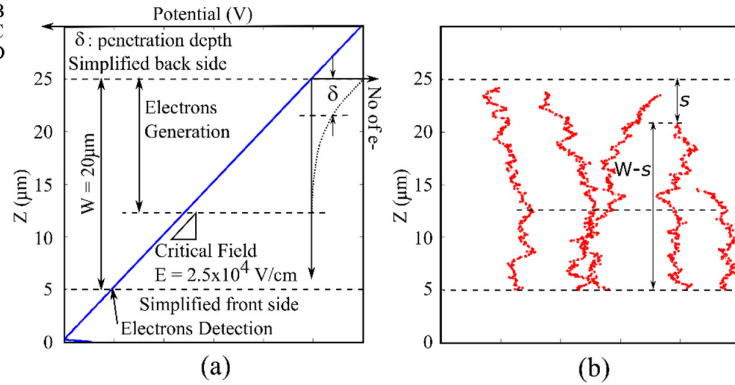


Fig. 3 The model for the derivation of the expression of the temporal resolution limit and the Monte Carlo simulations  
 (a) The conditions, (b) Example trajectories of signal electrons

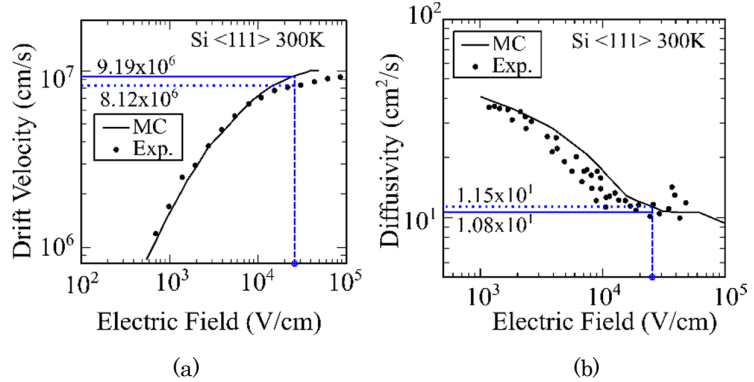


Fig. 5 Drift velocity (a) and diffusion coefficient (b) vs. Electric field: Intrinsic silicon <111> at 300 K  
 Dots: Data from experiments, Lines: Monte Carlo simulations with full-band calculations.